

Computational and Experimental Insights into Reactive Forms of Oxygen Species on Dynamic Ag Surfaces under Ethylene Epoxidation Conditions

A Thesis

Presented to

the faculty of the School of Engineering and Applied Science

University of Virginia

in partial fulfillment
of the requirements for the degree

Master of Science

by

Changming Liu

July 2021

APPROVAL SHEET

This Thesis
is submitted in partial fulfillment of the requirements
for the degree of
Master of Science

Author Signature: Changming Liu

This Thesis has been read and approved by the examining committee:

Advisor: Christopher Paolucci

Committee Member: William Epling

Committee Member: Robert J. Davis

Committee Member: Leonid V. Zhigilei

Committee Member: _____

Committee Member: _____

Accepted for the School of Engineering and Applied Science:



Craig H. Benson, School of Engineering and Applied Science

July 2021

Abstract

Ethylene epoxidation, the selective oxidation of ethylene to ethylene oxide (EO), is one of the most important industrial processes because EO is a crucial intermediate for many desired chemicals. This reaction is catalyzed by supported Ag particles and has two competing reaction pathways: epoxidation to EO, or undesired complete combustion to CO_2 and H_2O . The selectivity toward EO is around 45% on unpromoted Ag, while it can go upwards of 85% with the inclusion of promoters. Despite years of study, the reactive intermediates, mechanism, and active phase of the catalyst are still heavily debated.

In this study, we use a combination of density functional theory (DFT) calculations and Raman Spectroscopy to investigate the dynamics and structure of the Ag surface and intermediates under reaction conditions. Our findings suggest that the active phase of the catalyst consists of several nanometers thick Ag_2O -like film on Ag bulk. This implies that under industrial conditions, EO formation is on a highly oxidized and reconstructed surface which cannot be fully represented by well-defined and low-coverage Ag surface models (e.g., Ag(111), Ag(110), Ag(100)). We propose that the structure, dynamics, and the prevailing reaction pathways upon Ag-based EO catalysts strongly depend on oxygen coverage and speciation.

Contents

1	Introduction	4
2	Methods	6
2.1	Surface Calculations	6
2.2	Ab initio Thermodynamics	7
3	Results	8
3.1	In situ Raman Spectra under Steady-state Ethylene Epoxidation	8
3.2	Computed Free Energies of O* and O ₂ * Containing Ag Surfaces . . .	11
3.3	Gibbs Free Energies and Frequencies for Dioxygen Species on an Oxide Slab Model	16
3.4	In Situ Raman during Oxidative Treatments of Ag and Ag ₂ O Nanopar- ticles	19
4	Conclusion	22

Acknowledgements

I would like to express my deep and sincere gratitude to my research advisor, Professor Chris Paolucci, for the dedicated support and guidance on my research and life. His enthusiasm, knowledge and sincerity have deeply inspired me. He patiently taught me to carry out the research, to present, and to write as clear as possible. It was an honor to work with him.

Beside my advisor, I would like to thank the rest of my thesis committee: Professor William Epling, for his humor and insightful questions in my past presentations; Robert J. Davis, for beautifully teaching me the fundamentals of reaction engineering; and Leonid V. Zhigilei, for letting me better understand atomistic simulations.

I would like to say thanks to my research colleagues, Keka Mandal, Anna Sviripa, Anukriti Shrestha, Asanka Wijerathne, and Sugandha Verma, for their patience, support and encouragement. I could not finish my study without their help. I would like to thank my collaborator, Devinda Wijewardena, for his effort into our project. I would like to thank my friends Chen Cai and Xutao Gao, for our enthusiastic, stimulating and joyful discussions about life and future.

I am grateful to my parents for their love, support, and sacrifices for educating and preparing me for my future. You are always there for me.

Chapter 1

Introduction

Ethylene oxide (EO) is used to produce ethylene glycol, ethoxylates, ethanolamines and a host of other intermediates and end-user products in textile, personal care and pharmaceutical industries[1, 2]. Industrially, EO is produced using Ag/ α -Al₂O₃ catalysts using air and C₂H₄ co-feed. The mechanistic pathway can be two-fold, one of which leads to EO formation and the other leads to CO₂ formation[3]. Despite this chemistry being extensively studied, the mechanism is still debated.

Different hypotheses exist pertaining to O species on Ag. Barteau et al., revealed the presence of a surface intermediate called an oxametallacycle (OMC), where C₂H₄ is bound to a surface O-atom and surface Ag site[4]. A subsequent study suggested that the two pathways diverge from the oxametallacycle. Based on kinetic isotope effect measurements, they have proposed that a 1,2-H shift is responsible for the isomerization from ethylene oxide to acetaldehyde, which results in the total combustion pathway[5]. Additionally, they performed theoretical calculations on the evolution of oxametallacycle intermediates on well-defined Ag surfaces[4, 6, 7]. However, the structures have relatively low O coverages, which diverges from the industrial reaction conditions.

Alternatively, van Santen et al. suggested a mechanism for EO formation on a Ag surface with high O content, which they modeled using the Ag₂O (001) surface[8, 9]. On this surface, the first pathway is a direct epoxidation of ethylene by an Eley–Rideal (ER) mechanism, where EO is the only primary product after ethylene directly adsorbs on the surface atomic O of the Ag₂O surface. The other possible pathway is oxametallacycle formation on surface O vacancies on Ag₂O (001), leading to divergent pathways forming EO and CO₂, similar to EO and acetaldehyde formation on Ag (111) surface proposed by Barteau et al. [4].

Regardless of the mechanism of epoxidation, literature suggests that subsurface O atoms help in increasing the selectivity to EO by causing surface O atoms to become more electrophilic[10, 11, 12, 13]. For instance, Rocha et al. identified multiple types of surface O species via X-ray photoelectron spectroscopy (XPS), and found that more electrophilic O (O1s > 530 eV) correlated with a higher selectivity to EO, and high electrophilic O is related to high O* concentrations on the Ag surface[14]. More electrophilic O is proposed to favor epoxidation over combustion pathways[15, 16]. However, such proposals are based on the OMC mechanism, where the selectivity is indirectly determined by the O coverage[5, 7, 4]. More specifically, the change in the selectivity is caused by the change in the potential energy surface (PES) induced by a different O coverages. In contrast, the ER mechanism proposed

by van Santen et al.[8, 9] has different types of active sites where ethylene reacts with surface O* on Ag₂O (001) with a perfect selectivity to EO. The non-selective pathway is initiated by O-vacant sites (*) on Ag₂O (001) surfaces.

Compared to other spectroscopic methods (e.g. XPS, high-resolution electron energy loss spectroscopy, Fourier transform infrared spectroscopy), surface enhanced Raman spectroscopy (SERS) can be operated *in situ*, under EO epoxidation conditions (atmospheric pressure, around 500 K) while having the capability of probing oxidized (and potentially highly reconstructed) Ag layers. Thus, SERS features are widely used to study O₂ adsorption on Ag surfaces[17, 18, 19, 20, 21, 22, 23]. Yet, there are a limited number of experimental SERS studies for ethylene epoxidation, and assignments from SERS remain controversial, especially around 800 cm⁻¹. This band is important because it has been shown to correlate with ethylene epoxidation selectivity[14, 24]. The 800 cm⁻¹ frequencies have been assigned to two contradictory O-related species: atomic O[19, 20] or diatomic O[21, 25, 17]. There is relatively less information related to calculated frequencies of surface O-related species, which makes it more challenging to resolve the 800 cm⁻¹ controversy.

Here, we have analyzed the thermodynamics of Ag_xO_y structures across a wide range of O coverages using density functional theory (DFT). We also performed frequency calculations on the lowest energy structures and compare with frequencies acquired from experimental Raman Spectroscopy. Experimentally, our collaborators at UIUC used steady-state SERS to study the surfaces under O₂ and C₂H₄ co-feed conditions and in O₂ alone. We found that the active phase of the catalyst consists of a several nanometers thick Ag₂O-like film on Ag bulk. This implies that under industrial conditions, the Ag surface is highly oxidized. We also propose that surface intermediates responsible for the 800 cm⁻¹ band, and potentially reaction pathways, are strongly correlated with oxygen coverage.

Chapter 2

Methods

We performed DFT calculations with the Vienna Ab initio Simulation Package (VASP version 5.4.4)[26] and the GGA-PBE[27] exchange-correlation functional. All calculations were non-spin-polarized and used a plane wave cutoff energy of 400 eV and the projector augmented wave (PAW) method for core-valence interactions[28, 29]. Bulk fcc Ag ($Fm\bar{3}m$) and Ag₂O ($Pn\bar{3}m$) structures were taken from the Materials Project database[30], and their geometries and cell vectors were subsequently optimized using 10^{-8} eV and 0.01 eV/Å for energy and force convergence criteria, respectively. The k-points and lattice parameters used for bulk Ag and Ag₂O are reported in Table 2.1.

Table 2.1: k -points and lattice parameters for bulk Ag and Ag₂O

Structure	a	b	c	K-point Mesh	Ag Atoms	O Atoms
Bulk Ag	4.117	4.117	4.117	(9, 9, 9)	4	0
Bulk Ag ₂ O	4.841	4.841	4.841	(6, 6, 6)	4	2

2.1 Surface Calculations

The asymmetric Ag_xO_y surfaces proposed by literature were generated through Atomic Simulation Environment (ASE) package[31] and Python Materials Genomics (pymatgen)[32]. Additionally, for each Ag facet we sampled surfaces with O adsorbed on symmetrically unique sites[33, 34] at coverages varying from 0.11 to 0.44 monolayers (ML). For the Ag_xO_y calculations, we used the k-point density from the k-points per reciprocal Å for Ag bulk in the x and y directions (rounded up), and a single k-point in the z direction. At least 12 Å of vacuum was added for all surface calculations. Surfaces were optimized to a convergence criteria of 10^{-6} eV and 0.03 eV/Å. All asymmetric slabs had at least four layers of Ag atoms, with the two bottom layers fixed. We calculated harmonic vibrational frequencies for surfaces by numerical differentiation of atomic forces with 0.015 Å displacements. For computational efficiency of Ag_xO_y frequency calculations, only the top two to three layers in the structures were allowed to relax.

2.2 Ab initio Thermodynamics

To relate calculated Ag_xO_y energies to experimental conditions, we used *ab initio* thermodynamics to compute the free energy[35]:

$$\gamma(T, p) = (E_{\text{DFT}} - E_{\text{ref}} - N_{\text{Ag}}\mu_{\text{Ag}} - N_{\text{O}}\mu_{\text{O}})/A \quad (2.1)$$

where γ is the free energy, A and E_{DFT} are the surface area and total energy of the Ag_xO_y slab, respectively. E_{ref} is the total energy of the Ag slab, N_{Ag} is the difference in the number of Ag in the Ag_xO_y slab compared to the Ag slab, μ_{O} is the chemical potential for oxygen, and μ_{Ag} is the chemical potential for Ag, which we define as the energy of an Ag atom in the Ag bulk. We related μ_{O} to the pressure of $\text{O}_2(\text{g})$ as follows:

$$\mu_{\text{O}} = \frac{1}{2} \left(E_{\text{O}_2} + \tilde{\mu}_{\text{O}_2}(T) + kT \ln\left(\frac{p_{\text{O}_2}}{p^\circ}\right) \right) \quad (2.2)$$

Here, E_{O_2} is the calculated energy of an isolated O_2 molecule, $\tilde{\mu}_{\text{O}_2}$ is calculated using the NIST JANAF Thermochemical tables[36], and p° is the standard state pressure (0.1 MPa).

Chapter 3

Results

3.1 In situ Raman Spectra under Steady-state Ethylene Epoxidation

Silver nanoparticles form ethylene oxide when in contact with O_2 and C_2H_4 reactants at temperatures between 423 - 543 K[37]. Figure 3.1 shows Raman spectra acquired by our collaborators at UIUC under distinct combinations of O_2 and C_2H_4 pressures at 523 K (Figure 3.1a, 2 kPa O_2 , 0.5 - 9.8 kPa C_2H_4 ; Figure 3.1b, 2 kPa C_2H_4 , 2 - 80 kPa O_2). In Figure 3.1a, with $C_2H_4:O_2$ ratio ≤ 1 , an asymmetric feature with a peak at 820 cm^{-1} and a broad shoulder extending to around 950 cm^{-1} remains controversial with prior investigations attributing this feature either to dioxygen surface species (e.g., O_2^{2-} , O_2^-)[21, 25, 17] or to different forms of O^* on or near the surface[38, 39, 20]. Figure 3.1a also shows that these features attenuate and new peaks emerge upon C_2H_4 (0 - 9.8 kPa C_2H_4 , 2 kPa O_2 , He as balance, 523 K). The feature at 820 cm^{-1} is absent when ratios of $[C_2H_4]$ to $[O_2]$ exceed unity, and the disappearance of this peak correlates with the appearance of peaks at 220 cm^{-1} , 640 cm^{-1} and broad features near 1300 cm^{-1} and 1600 cm^{-1} . Furthermore, the intensity of peaks above 1250 cm^{-1} become more significant with increases in $[C_2H_4]$. Figure 3.1b presents spectra obtained at fixed $[C_2H_4]$ (2 kPa C_2H_4) but across a range of $[O_2]$ (2 - 80 kPa O_2) at 523 K. The trends in the growth and attenuation of Raman active features as functions of the ratio of $[O_2]$ to $[C_2H_4]$ agree with those in Figure 3.1a, which suggests these surfaces are predominantly saturated with O_2 - and C_2H_4 -derived intermediates and negligible numbers of unoccupied sites. The features at 820 , 910 , and 990 cm^{-1} , that decreased in intensity with increasing $[C_2H_4]:[O_2]$ ratios in Figure 3.1a, begin reappearing and increasing in intensity once $[O_2]:[C_2H_4]$ ratio exceeds 4. With the exception of the 350 cm^{-1} and 820 cm^{-1} features (which increase in intensity), the other peaks under 700 cm^{-1} begin attenuating when $[O_2]:[C_2H_4]$ ratio exceeds 4.

The response of the Raman features in Figure 3.1 to reactant pressures give strong evidence that monoatomic and potentially diatomic forms of oxygen coexist with organic species on Ag catalyst surfaces at $[C_2H_4]$ to $[O_2]$ ratios of 1 - 5 (C_2H_4 rich) and 0.025 - 1 (O_2 rich), and temperatures (473 K - 573 K) commonly used for industrial ethylene epoxidation [40, 41]. Prior investigations utilizing infrared[25, 42], high-resolution electron energy loss[4], and Raman spectroscopy[38, 39, 23] to characterize the surface species formed with contact of these reactants or ethylene oxide with Ag nanoparticles or single crystal surfaces (see Table 3.1) allow us to

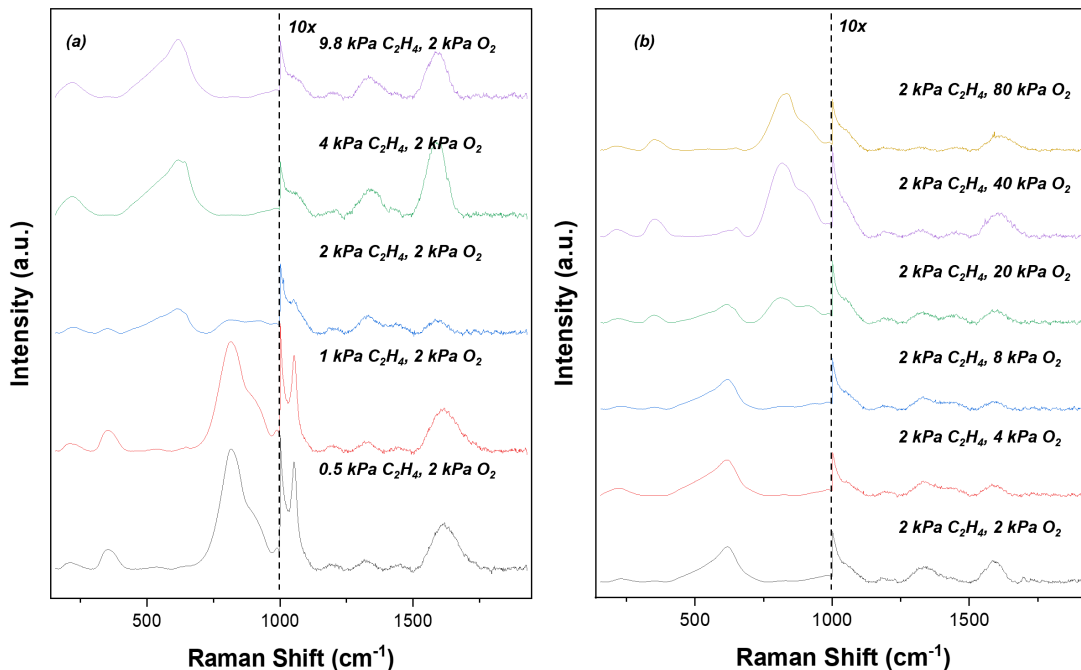


Figure 3.1: Steady-state Raman spectra of surface and subsurface species formed on Ag nanoparticles with reactant mixtures of (a) fixed O_2 pressure (2 kPa O_2) and increasing C_2H_4 pressures (0 – 10 kPa C_2H_4); and (b) fixed C_2H_4 pressure and increasing O_2 pressure (0 – 80 kPa O_2), at 523 K. In each spectrum, above 1000 cm^{-1} , the peak intensities were multiplied by 10 for greater clarity. Experimental conditions: Temperature = 523 K and 1 atm.

tentatively assign several of these features.

As seen in Table 3.1, features at 350 cm^{-1} appear to relate to surface atomic O^* . The broad feature with a peak between $810 - 830 \text{ cm}^{-1}$ present on contact with an excess of O_2 lies at a frequency uncharacteristically high for forms of O^* -atoms either at low coverages on metallic transition metal [17, 25], for high coverage ad-layers, or for reconstructed surface oxides[43, 44, 45]. Consequently, we favor early proposals[46] that have similar vibrational frequencies on electrolytic Ag films, supported Ag nanoparticles, and Ag single crystals, and assigned this band to diatomic oxygen species[47, 17, 25, 21]. Finally, the broad peaks between 1300 and 1700 cm^{-1} are consistent with stretching and bending modes of C_2H_4 . The assignment for the band between $500 - 700 \text{ cm}^{-1}$ is also controversial as shown in Table 3.1. Moreover, our steady-state Raman spectra show that as the ratio of $[\text{C}_2\text{H}_4]$ to $[\text{O}_2]$ increases, the $500 - 700$ band strengthens, implying this band may originate from ethylene or EO rather than being the proposed $\nu(\text{Ag-O}_{\text{subsurface}})$ or $\nu(\text{Ag-O}_2)$.

The contributions of surface intermediates with distinct dependence of their coverages on the pressures of C_2H_4 and O_2 to the spectral features shown in Figure 3.1 are deconvoluted using multivariate curve resolution alternating least squares (MCR-ALS, Figure 3.2). Component one increased with increasing $[\text{O}_2]:[\text{C}_2\text{H}_4]$ ratios and contains the broad and dominant peak at 820 cm^{-1} , as well as the shoulder extending to 920 cm^{-1} and peaks at 350 and 990 cm^{-1} . Therefore, we assign this component to signify adsorbed molecular O_2 and atomic O . Components two and three both contain a peak at 640 cm^{-1} . Prior studies would suggest that component two and component three correspond to structures containing subsurface atomic oxygen close

Table 3.1: Plausible Peak Assignments from Experiments in Literature

Raman Frequency Band (cm^{-1})	Literature Proposed Frequencies (cm^{-1})	Proposed Vibrational Modes
220	240	$\nu(\text{Ag-O}_2)$ [42]
	270	$\nu(\text{Ag-O}_{\text{surface}})$ [43]
350	325	$\nu(\text{Ag-O}_{\text{surface}})$ [42]
	351	$\nu(\text{Ag-O}_{\text{surface}})$ [36,44]
	335	$\nu(\text{Ag-O}_{\text{surface}})$ [45]
640	622	$\nu(\text{Ag-O}_2)$ [44]
	640	$\nu(\text{Ag-O}_{\text{subsurface}})$ [12]
	630	$\nu(\text{Ag-O}_{\text{subsurface}})$ [13]
	676	$\nu(\text{Ag-O}_2)$ [46]
	622	$\nu(\text{Ag-O}_2)$ [47]
810	697	$\nu(\text{Ag-O}_2)$ [11]
	802	$\nu(\text{Ag-O}_{\text{subsurface}})$ [11]
	800	$\nu(\text{Ag-O}_{\text{surface}})$ [12]
	803	$\nu(\text{Ag-O}_{\text{surface}})$ [13]
	810	$\nu(\text{Ag-O}_{\text{surface}})$ [15]
	800	$\nu(\text{Ag-O}_{\text{surface}})$ [14]
	790	$\nu(\text{Ag-O}_{\text{surface}})$ [48]
990	805	$\nu(\text{Ag-O}_2)$ [49]
	983	$\nu(\text{Ag-O}_2)$ [44]
	954	$\nu(\text{Ag-O}_{\text{surface}})$ [50]
	956	$\nu(\text{Ag=O}_{\text{surface}})$ [14]
	995	$\nu(\text{Ag-O}_2)$ [46]
1340	983	$\nu(\text{Ag-O}_2)$ [47]
	1370	amorphous carbon[46]
1590	1360	amorphous carbon[15]
	1590	amorphous carbon[15]
	1596	amorphous carbon[46]

the bulk, or dioxo species. However, based on the evolution of the frequencies under different $[\text{C}_2\text{H}_4]$ to $[\text{O}_2]$ ratios in Figure 3.1, we tentatively assign these two components to C_2H_4 - or EO-related species. The correlation of the 810 cm^{-1} to lower wavenumbers (210 and 350 cm^{-1}) demonstrate that the Ag surface and near surface region must possess high contents of structures with atomic oxygen before the formation of the species represented by the 810 cm^{-1} feature becomes favorable (i.e., exergonic). Component four contains a feature at 790 cm^{-1} , in addition to peaks at 1200 , 1350 and 1590 cm^{-1} , which make appearances across multiple components. These results suggest that the forms of reactive oxygen species on the surface depend upon the reactant pressures. It also implies that distribution of oxygen present in low pressure studies often performed on model Ag surface (e.g., $\text{Ag}(111)$)[4, 5, 48, 11, 49, 50] and related calculations will differ significantly from those obtained at the reactant pressures implemented for ethylene epoxidation on supported Ag catalysts[43, 51, 52, 53]. These distinctions likely extend beyond differences in reactant coverages and could include catalytically significant variations in bulk phase of the Ag-based catalyst, the amount of subsurface oxygen (even in the absence of chlorine

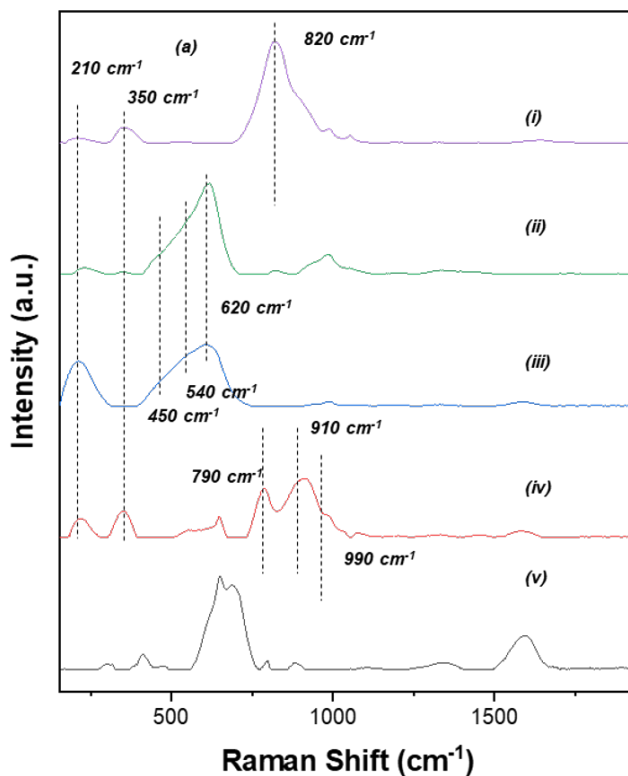


Figure 3.2: Principal components obtained from the 2 hr co-feed experiments shown in Figure 3.1. The principal components show how each individual component contributes to the overall shape of the spectra at a given moment.

and other promoters), and the appearance of surface reconstructions.

3.2 Computed Free Energies of O^* and O_2^* Containing Ag Surfaces

To address disagreements in the literature regarding assignments for Ag-O vibrations, we examined proposed models for Ag_xO_y surfaces. Before computing frequencies, we first evaluated the relative thermodynamic stability of different Ag_xO_y surfaces. We performed geometry optimizations on oxygen-containing reconstructed and unreconstructed Ag (111) and Ag (100) terraces, and Ag (110) and Ag (311) structures as a model for steps and edges, as shown in Figure 3.3.

For comparison to experimental conditions we computed the Gibbs free energy of each surface using equation 2.2. Surface phase diagrams as a function of $\Delta\mu_O$ for all computed models are shown in Figure 3.4 and 3.5. For the corresponding temperature and pressure related phase diagrams, Figure 3.6 and 3.7 show the lowest free energy structures as a function of temperature and O_2 pressure for each facet. We chose Ag_2O as the bulk oxide reference to estimate where the metal to metal-oxide phase transition occurs[51]. Bulk Ag_2O formation is not favorable at the experimental conditions used here (20 - 101 kPa oxygen pressure and temperatures 500 - 800 K). Therefore, we expect Ag_xO_y surfaces to be predominant.

Figure 3.6 reports the relative stability of Ag (111) surfaces; the Ag (111),

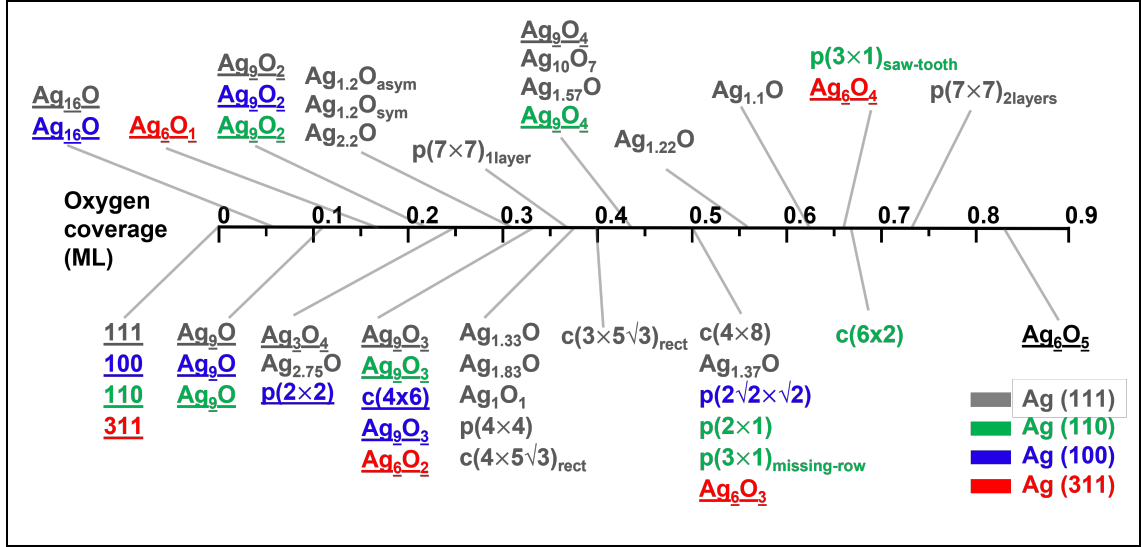


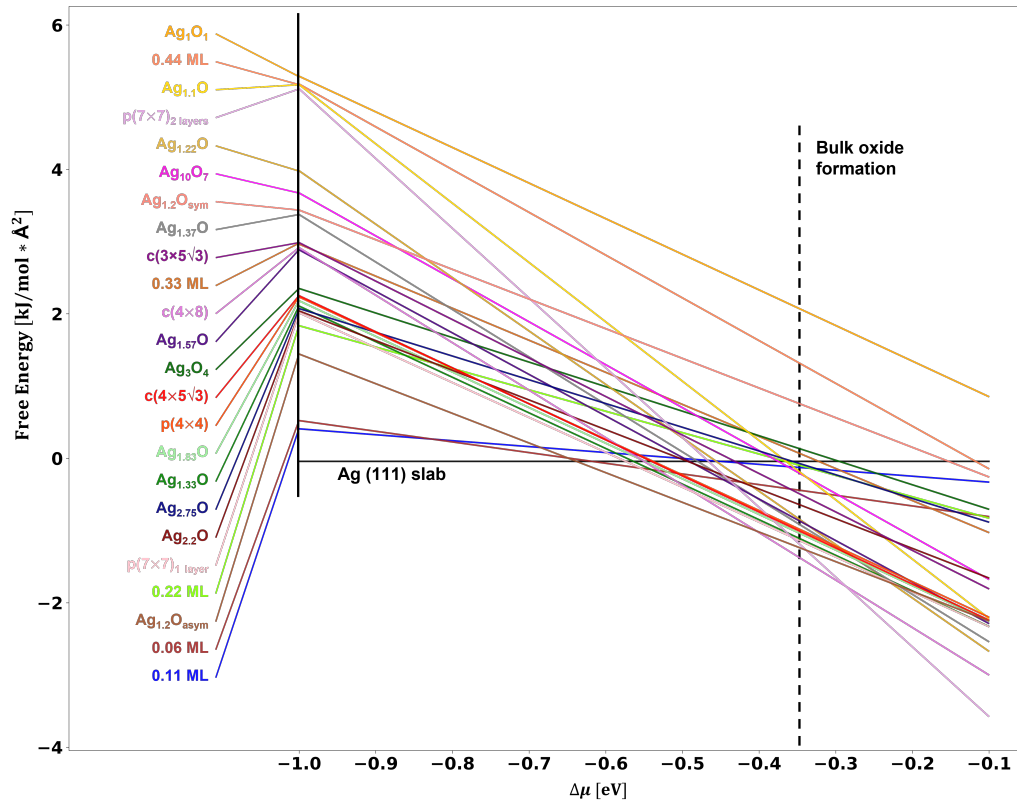
Figure 3.3: A summary of examined Ag_xO_y models from literature (without underline) and in-house generation (with underline) for the four facets. Oxygen coverage calculation is consistent with the work from Martin et al.[54].

$Ag_{1.2}O_{asym}$, and (111)- $c(4 \times 8)$ -O are the lowest energy surfaces at low, intermediate, and high oxygen coverages, respectively. The $Ag_{1.2}O_{asym}$ and Ag (111) are the lowest energy structures at 550K, 1-100 kPa O_2 partial pressure. There are several reported phase diagrams for Ag (111) in literature [55], however none of those contained all of the structures computed herein. Our prediction of relative stability for (111)- $c(4 \times 8)$ at $\Delta\mu = -0.4$ to -0.3 eV is consistent with Martin et al.[54], and the $Ag_{1.2}O_{asym}$ as a low-energy phase at range $\Delta\mu = -0.55$ to -0.4 eV is consistent with the prediction from Michaelides et al.[56] under the same range. We also included the proposed $Ag_{10}O_7$ and Ag_3O_4 structures from grand canonical Monte Carlo (GCMC) study from their ab initio phase diagram. However, these structures are not as stable as those in (111)-(T,p) phase diagram. The second most explored facet is Ag (110), with multiple proposed reconstructions under oxidizing conditions[11, 57, 58]. Figure 3.6b shows that as $\Delta\mu$ increases, the stable phase switches from (110)- $p(3 \times 1)$ -O, to (110)- $p(2 \times 1)$ -O, and finally to (110)- $c(6 \times 2)$ -O. The evolution of these species is consistent with the work from Jones et al. [44]. The predictions are also consistent with experimental LEED patterns of $p(2 \times 1)$ acquired by Campbell et al. under UHV conditions[11, 59, 60].

There are only a few studies in the literature for thermodynamically stable phases of Ag (100). Our computed stable surfaces were Ag (100), 0.11 monolayer (ML), 0.22 ML, 0.33 ML, and (100)- $p(2\sqrt{2} \times \sqrt{2})$ -O (Figure 3.7a). At $\Delta\mu = -0.55$ to -0.4 eV, the relative stability of the (100)- $p(2\sqrt{2} \times \sqrt{2})$ -O phase from our phase diagram is consistent with the phase diagram reported by Costina et al.[61], except for the (100)- $p(4 \times 6)$ -O and (110)- $c(6 \times 2)$ -O surfaces. We believe that these structures did not appear on our energy hull because they were less stable than the 0.22 ML and 0.33 ML structures we generated. To our knowledge, there are no reports of phase diagrams with Ag(311) available for comparison, and structures on Figure 3.7b are purely generated by us.

We performed vibrational frequency calculations for all the structures in the phase diagrams. Table 3.2 summarizes the calculated maximum frequency for each

(a) Linear phase diagram of all calculated Ag (111) structures.



(b) Linear phase diagram of all calculated Ag (100) structures.

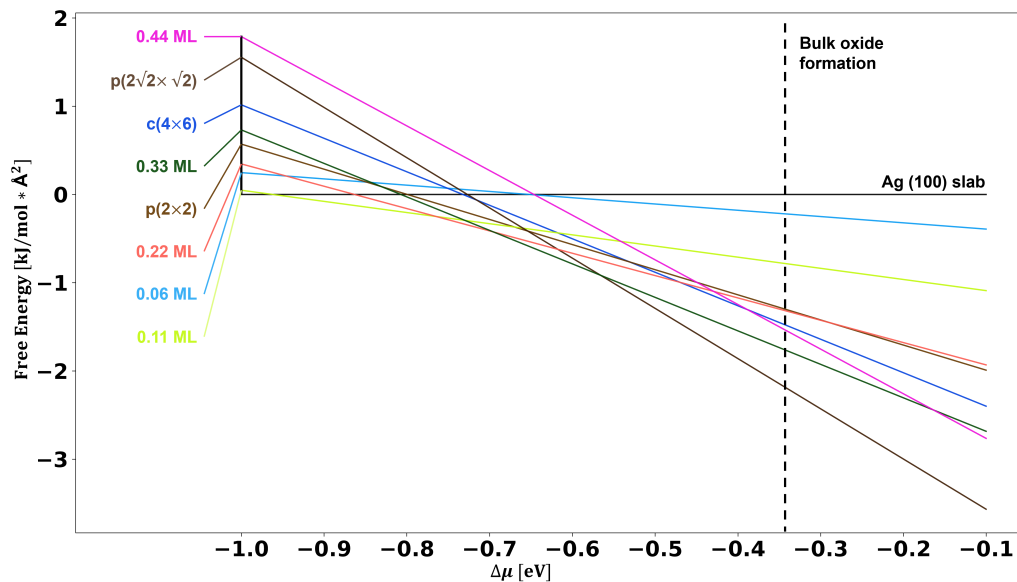
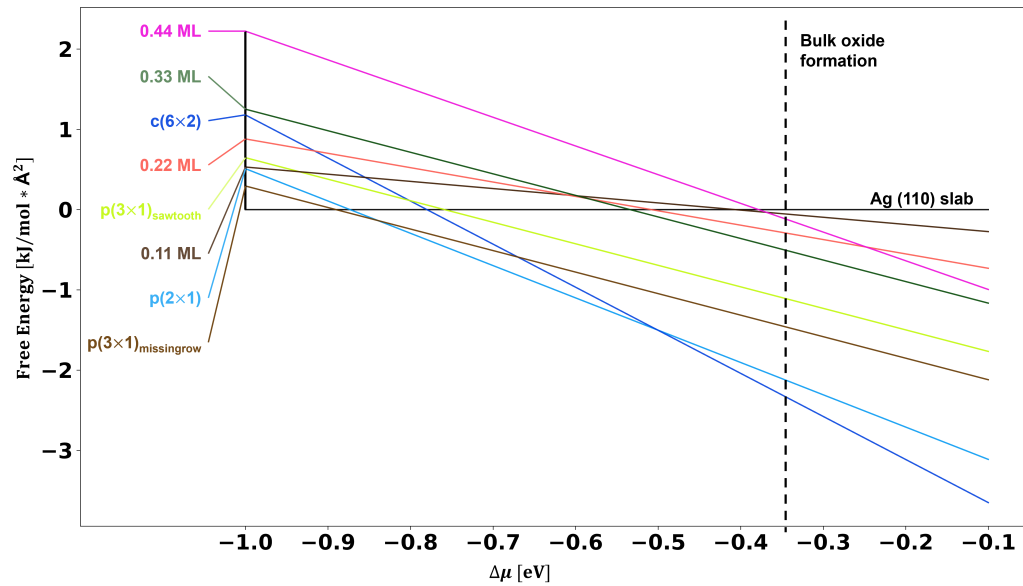


Figure 3.4: Linear phase diagram of Ag (111) and Ag (100).

(a) Linear phase diagram of all calculated Ag (110) structures.



(b) Linear phase diagram of all calculated Ag (311) structures.

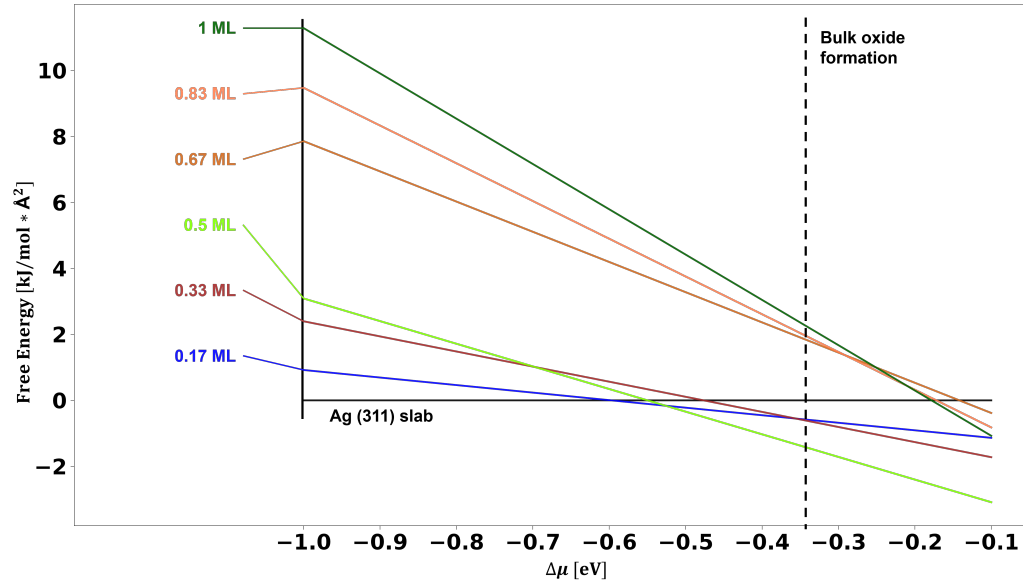


Figure 3.5: Linear phase diagram of Ag (110) and Ag (311).

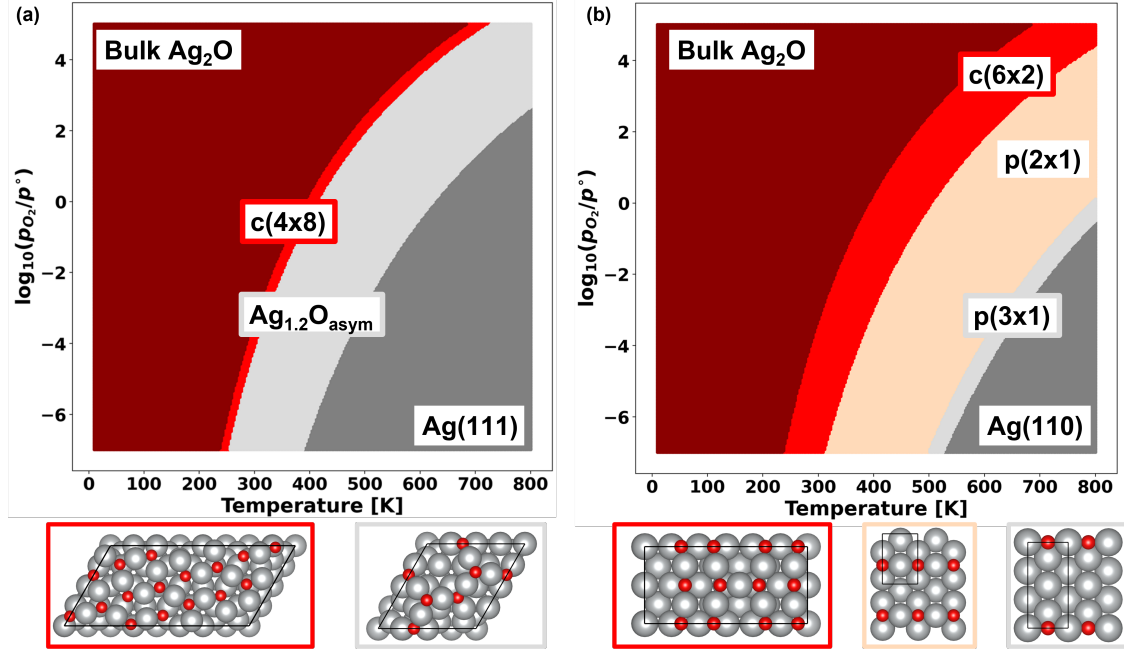


Figure 3.6: Ab initio phase diagram for the (a) Ag (111)–O system and (b) Ag (110)–O system. Below each phase diagram are the corresponding structures, and the black line in each structure marks the computed unit cell. O atoms are in red color and Ag atoms are in silver colors.

structure. For all four facets, the computed frequencies were below 600 cm^{-1} . Our results are similar to the frequency calculations for Ag(111) surface models with surface and subsurface oxygen adsorption computed by Li et al[62]. They observed a range of vibrational frequencies from 200 cm^{-1} to 526 cm^{-1} , with the latter being maximum frequency acquired from a subsurface O. To summarize, the proposed low energy models in our phase diagram do not explain the 800 cm^{-1} frequency observed by us or other groups with the *in situ* Raman measurements[38, 22].

However, the models discussed above only represent various types of atomic and subsurface oxygen (as the 1st and 3rd layers of the O-Ag-O tri-layer system in (111)-c(4×8) structure). Thus, we decided to explore the Ag dioxo species as a potential explanation for this peak. We generated Ag dioxo species starting from the reconstructed and unreconstructed Ag surfaces that appear on our phase diagrams, as shown in Table 3.3. When generating these species, we tried two schemes regarding the O coverage of generated guesses: equal and higher coverage against the original reconstructed structures. The equation for computing reaction free energies is shown below:

$$G(T, p) = E_{\text{ref}+x\text{O}} - E_{\text{ref}} - xN_{\text{O}}\mu_{\text{O}} \quad (3.1)$$

where G is the Gibbs free energy, T and p are the temperature and pressure, E_{ref} is the structure on the energy hull, and x is the number of additional oxygen included for generating dioxo structures. Depending on the schemes, x can be either 0 or 1. For example, $x = 0$ when we move two different O atoms in the structure close to each other (to around $1.4 - 1.5\text{ \AA}$) and form a dioxo species, and $x = 1$ when we add an additional O atom to one of the existing and symmetrically unique O

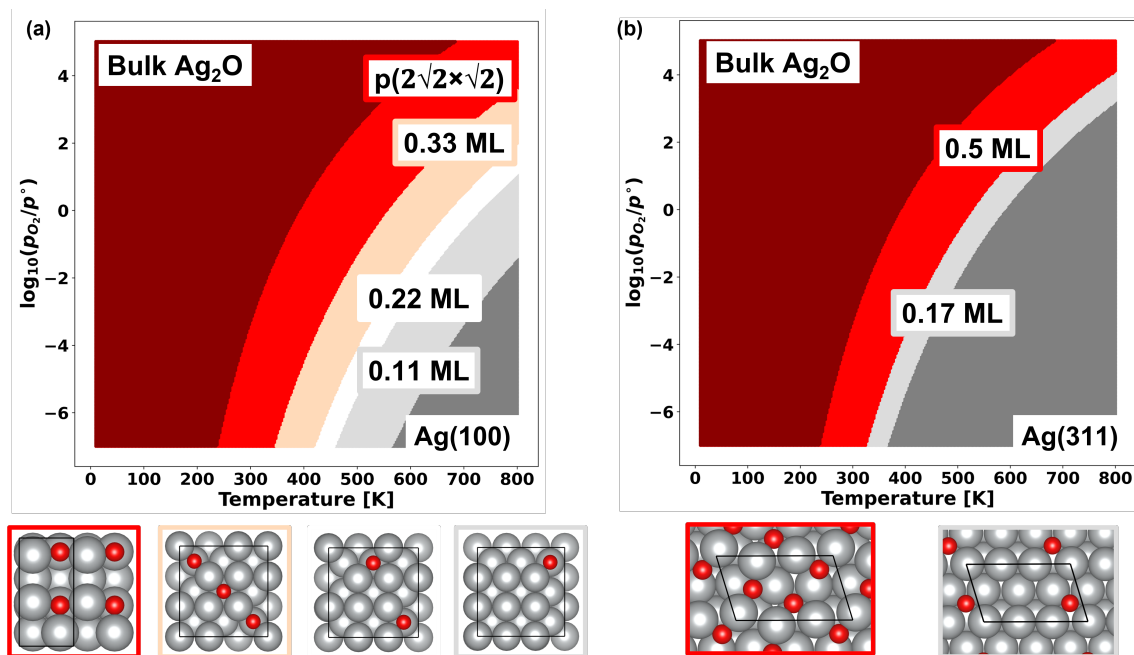


Figure 3.7: Ab initio phase diagram for the (a) Ag (110)–O system and (b) Ag (311)–O system. Below each phase diagram are the corresponding structures, and the black line in each structure marks the computed unit cell. O atoms are in red color and Ag atoms are in silver colors.

atoms. For all the generated dioxo species, the computed reaction free energies are endergonic. Therefore, we exclude the possibility of dioxo like species forming on proposed metallic and reconstructed surfaces.

Based on the evidence presented above, we conclude that the 800 cm^{-1} peak does not arise from atomic surface or subsurface O, or adsorbed dioxo species on the metal and reconstructed surfaces. However, we noticed a general trend for the structures in Table 3.3: except for (110)- $p(3 \times 1)$, for all the other structures, the calculated reaction energies decrease as the O coverage goes higher. This prompted us to explore Ag_2O -like film models with higher O coverages proposed by Ozbek et al.[8]. STM images from Derouin et al.[63] showed a development of bulk-like Ag_2O thin film with atomic oxygen dosing on Ag (111) surface at 500 K. Additionally, Heine et al.[64] showed that after exposing Ag (111) surface to 1.3×10^{-3} kPa oxygen, O1s had similar binding energy to that in Ag_2O , which suggested the formation of Ag_2O . Bukhtiyarov et al.[43] also concluded that a surface Ag oxide ($\text{Ag}_{2\pm 0.2}\text{O}$) was formed from Ag 3d 5/2 XPS data. Based on the evidence, we think an Ag_2O -like surface thicker than the widely discussed Ag_2O tri-layer surface may be formed under oxidizing conditions.

3.3 Gibbs Free Energies and Frequencies for Dioxygen Species on an Oxide Slab Model

We explored the formation of dioxo-like species on the oxide slab model at different O precoverages (Here, the precoverage is the original O coverage before we generate any dioxo species.) with DFT. Previously, adsorption energies of atomic O or molecular

Table 3.2: Calculated max frequencies of all structures on the energy hull for (111), (110), (100), and (311) facets.

Structure	Facet	Max calculated frequency (cm^{-1})
p(2×1)	110	600
p(3×1)	110	584
p($2\sqrt{2} \times \sqrt{2}$)	100	562
p(6×2)	110	555
1/2 ML	311	515
c(4×8)	111	512
Ag _{1.2} O _{asym}	111	500
2/9 ML	100	477
1/3 ML	100	422
1/6 ML	311	312
1/9 ML	100	304

Table 3.3: Calculated formation energies and free energies (523 K, 1 atm O₂) for the structures on the energy hull from (T, p) phase diagrams

Facet	Structure	Oxygen Change	Calculated Free Energies (eV)	Calculated Reaction Energies (eV)
111	c(4×8)	0	1.9	1.38
		1	1.23	0.71
	Ag _{1.2} O _{asym}	0	2.34	1.82
		1	2.06	1.53
110	c(6×2)	1	1.17	0.65
		0	1.87	1.35
	p(2×1)	4	1.35	0.83
		4	1.88	1.36
	p(3×1)	1	1.43	0.91
		2	1.9	1.38
100	p($2\sqrt{2} \times \sqrt{2}$)	1	1.44	0.92
		0	1.62	1.1
	0.11 ML	1	0.85	0.32
	0.22 ML	1	1.05	0.53
	0.33 ML	1	1.61	1.09
311	0.17 ML	1	0.8	0.28
	0.5 ML	1	1.23	0.71
	0.5 ML	0	1.22	0.70

O₂ on Ag₂O (001) surfaces with varying atomic O precoverages were reported[65], which will be discussed in the next paragraph. We systematically examined the symmetrically unique combinations of the three species (O vacancy, atomic O, and O₂) on four surface sites of (2×2) Ag₂O (001) surface with 5 layers. To disrupt the symmetry of the structure and enable sampling of different local minima, we methodically distorted the surface atoms and optimized the structures subsequently. Gibbs free energies were calculated at T = 523 K and 1 atm O₂ pressure:

$$G(523 \text{ K}, 1 \text{ atm O}_2) = E_{\text{Ag}_2\text{O}+x\text{O}} - E_{\text{Ag}_2\text{O}} - xN_{\text{O}}\mu_{\text{O}} \quad (3.2)$$

where G is the Gibbs free energy, $E_{\text{Ag}_2\text{O}}$ is the Ag₂O (001) surface, and x is the number of additional oxygen included for generating dioxo structures; x can range from -4 (four vacancies) to 4 (four dioxo species). For each specific configuration, we picked the lowest energy structure and computed frequencies (Figure 3.8). Here, we report frequencies of each dioxo species on the surface (e.g. slabs with 2 dioxo structures have 2 frequencies associated with them).

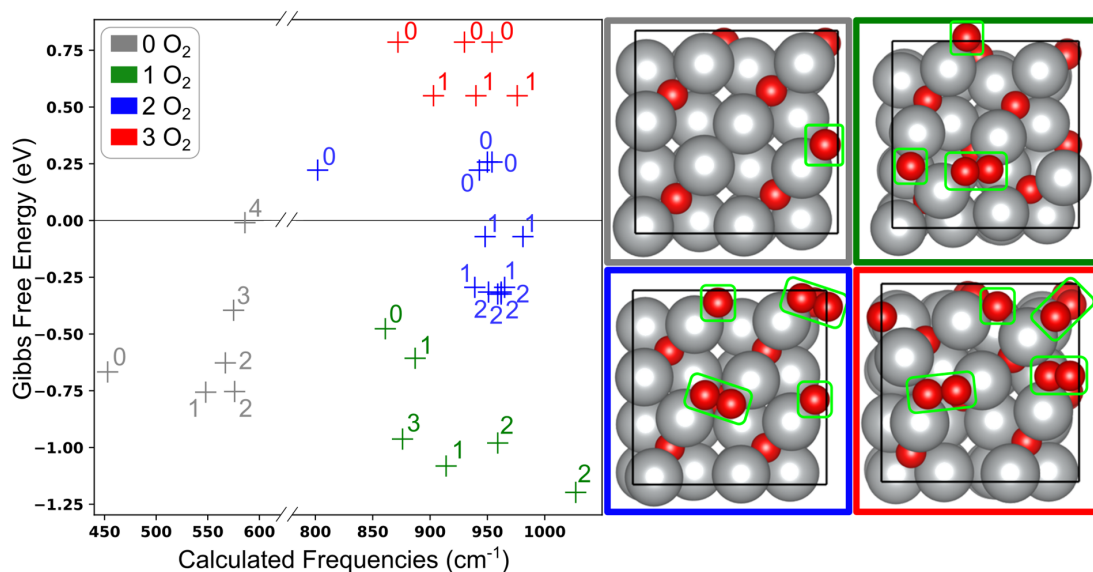


Figure 3.8: Left panel - Gibbs free energies (523 K, 1 atm O₂) and frequencies for varying surface coverage of O vacancies, atomic O and O₂ species on (2 × 2) Ag₂O (001) surface. Each structure has four adsorption sites; colors represent the number of dioxygen species and values are the number of atomic O; the remainder of the sites are O vacancies. Right panel – lowest energy structures for each dioxygen coverage; O and O₂ surface species are highlighted with bright green boxes.

Oxide slabs that only contain adsorbed atomic O and/or vacancies exhibited frequencies below 600 cm⁻¹, in agreement with previous observations for atomic O on metallic, reconstructed and unreconstructed surfaces in the previous section. However, when one or more dioxygen structures are present on the surface, we observe a multitude of structures with favorable Gibbs free energies and frequencies above 800 cm⁻¹. Comparing our results to the work from Ozbek et al[8], we noticed that their calculated adsorption energies of O₂ on oxide surfaces are much more endothermic (-6 kJ/mol for 0.5 ML precoverage and 255 kJ/mol for 0.75 ML precoverage).

Figure 3.9 summarizes the frequency calculations for structures based on Ag and Ag₂O surfaces. We found frequencies ranging between 802 - 1027 cm⁻¹ that correspond to dioxygen structures, which are in general agreement with the peak ranges for deconvoluted Raman component 1 in Figure 3.2. The experimentally observed broad peak at around 800 cm⁻¹ suggests a distribution of the species, potentially stemming from different coordination and orientations of the species across different sites. However, the majority of computed dioxygen containing surfaces reside in the 850 - 1000 cm⁻¹ range, which is a notable shift compared to the experiments. The exact oxide film surface structure is unknown, and, as with van Santen, our Ag₂O (001) slab is only an approximation of the oxide film that encapsulates the Ag particles. Therefore, the shift in frequencies could be due to the real catalyst surface having not being stoichiometric and/or due to the strain created by the lattice mismatch at oxide and metal interfaces.

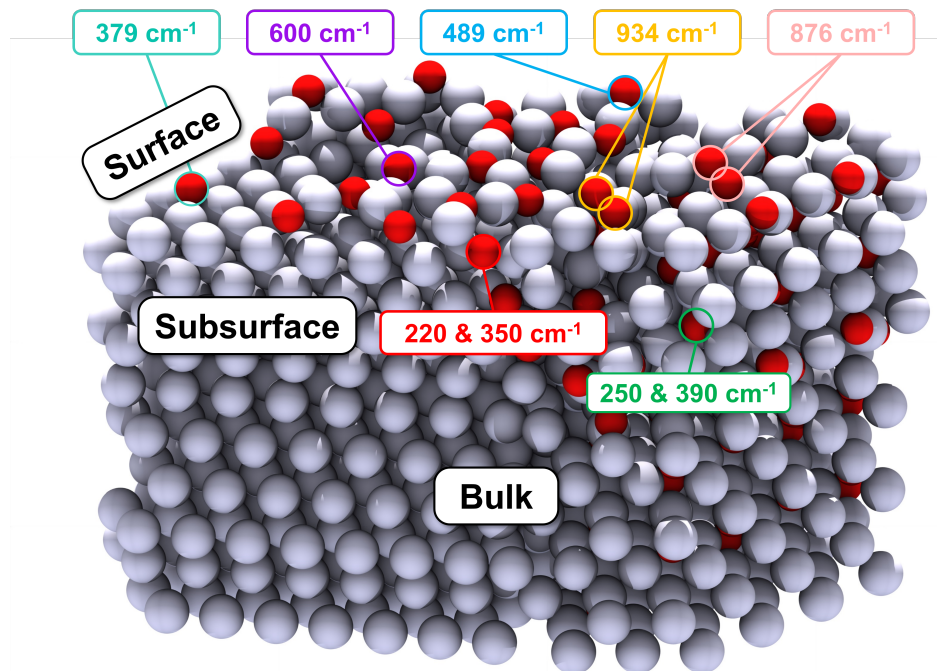


Figure 3.9: A summary of proposed (Ag-O) and (O-O) vibrational modes. The wavenumbers are from frequency calculations of different structures. This scheme does not predict the accurate structure of Ag or Ag₂O surfaces under reaction conditions.

3.4 In Situ Raman during Oxidative Treatments of Ag and Ag₂O Nanoparticles

Our calculations show that the energies of O-related species depend heavily on the stoichiometry and structure of Ag and Ag₂O surfaces. Experimentally, our collaborators compared the Raman spectra obtained from (initially) metallic Ag and polycrystalline Ag₂O nanoparticles. Figure 3.10 shows steady-state spectra acquired by placing pelletized Ag or Ag₂O nanoparticles within the *in situ* Raman cell and heating first to 523 K, and then to higher temperatures (523 – 673 K) before returning to 523 K.

Raman spectra of the Ag nanoparticles (Figure 3.10a) change noticeably during the oxidative treatments. After initial heating to 523 K, the sample does not possess any features that correspond to oxygen species. Multiple peaks at lower wavenumbers (220 cm⁻¹, 350 cm⁻¹, and 500 cm⁻¹) and an intense peak at around 845 cm⁻¹ appear upon heating to higher temperatures (573 - 673 K), which shows the formation of several different forms of oxygen. Subsequently, the relative intensities of all oxygen related features remain nearly constant upon reducing the sample temperature to 523 K, indicating that the changes caused by the oxidative treatment are irreversible at these conditions.

In contrast, Figure 3.10b shows that the Raman spectra for the Ag₂O sample remains nearly unchanged throughout the same series of oxidative treatments. The initial spectrum obtained possesses an intense scattering feature at 995 cm⁻¹, a broad peak that extends from 200 – 500 cm⁻¹, and smaller features at 615 cm⁻¹, 840 cm⁻¹, and 1080 cm⁻¹ (101 kPa O₂, 523 K), and these peaks undergo insignificant

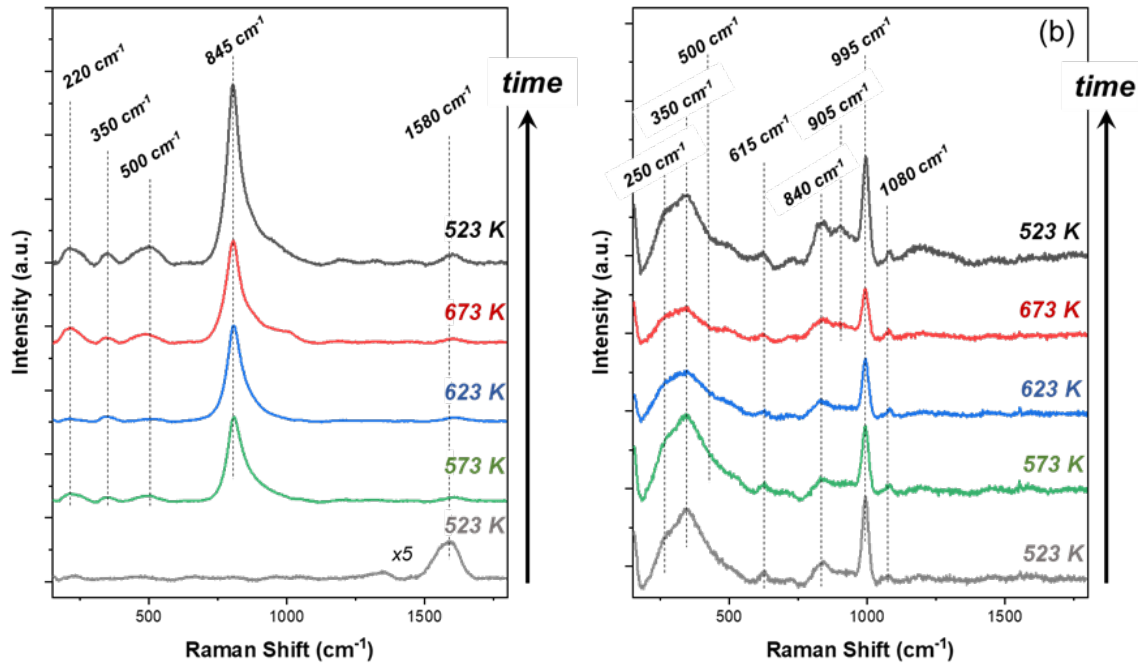


Figure 3.10: Steady-state Raman spectra obtained from (a) initially reduced Ag nanoparticles, and (b) Ag_2O nanoparticles. Materials were heated from ambient temperature to incrementally greater temperatures as indicated within flowing oxygen (101 kPa O_2).

changes when the sample is annealed at higher temperatures.

The comparison provides insight to the significance of the changes in the Ag nanoparticles during oxidation but also raises further questions. First, we observed the similarities in frequencies ($220\text{-}250\text{ cm}^{-1}$, 350 cm^{-1} , 500 cm^{-1} and $840\text{-}845\text{ cm}^{-1}$) between Figure 3.10a and 3.10b. This suggests that under oxidation conditions, the surface looks similar to the oxide, which justifies the computational models of Ag_2O (001) and our initial assignment of 850 cm^{-1} band to dioxo species. Second, the appearance of Raman features between $200 - 500\text{ cm}^{-1}$ represent high coverage of atomic oxygen both at and beneath the surface of Ag nanoparticles (Figure 3.10a); however, these features do not match the intensity or line shape of the comparable range of the spectra obtained from Ag_2O nanoparticles (Figure 3.10b). This indicates that the surface and near-surface region (around 2 nm) of the Ag nanoparticles contain significant amounts of oxygen but the bulk of the nanoparticles remain reduced following these treatments (101 kPa O_2 , 523 – 673 K, cumulative 15 h). Third, the spectra of Ag_2O appear similar before and after oxidative treatments (Figure 3.10b), especially below 650 cm^{-1} where prior investigations consistently assign Raman peaks to structures that involve atomic oxygen including those within the bulk of the nanoparticle[38, 39, 20, 46]. Fourth, the small changes that do appear only involve oxygen species with features at frequencies greater than 800 cm^{-1} . Intuitively, these thermal treatments cannot increase the oxidation state or bulk oxygen content of Ag_2O ; therefore, the appearance of these features reflect the evolution of the surface structure or composition. In summary, Figure 3.10a does not show the same quantity of subsurface O or a distribution of diatomic surface oxygen (peroxide or superoxide at range $800 - 1080\text{ cm}^{-1}$). Together with the calculated frequency differ-

ence of O-related species on Ag and Ag₂O surfaces illustrated in Section 3.3 and 3.2, we conclude that neither metallic Ag nor Ag₂O models used in prior investigations accurately represent the structure of the active EO catalyst.

Chapter 4

Conclusion

In this thesis, we performed DFT calculations, and combined with SERS from our collaborators, used these to study Ag surfaces under reaction conditions. Our DFT calculations on the Ag surfaces helped us develop a better understanding on multiple regions of Raman signals from our SERS spectra: a) lower wavenumbers regions (220 cm^{-1} and 350 cm^{-1}) are atomic oxygen species, b) the band at $600 - 700\text{ cm}^{-1}$ is more likely to originate from C_2H_4 or EO rather than atomic or molecular O, and c) the 800 cm^{-1} feature forms under high O coverages and we assign it to dioxo species. The summarized calculated frequencies from Section 3.2 and 3.3 are shown in Scheme 3.9. Under reaction conditions with C_2H_4 , we see that an inter-conversion between different atomic O species occur on the Ag surface. We propose that under reaction conditions, the phase of the catalyst is a surface oxide that likely contains several layers of atomic O species to the Ag bulk.

Our study helped us better know the surface structures and dynamics of ethylene epoxidation under reaction conditions. Yet, we lack the information about the barriers of the formation of a dioxo species on the Ag oxide surface, the barriers of surface O diffusion to the bulk under various O coverages, and the barriers of the formation of EO or acetaldehyde from O sites or vacancies. Moreover, the role of the halide promoter Cl has yet been probed yet, as well as the change of the barriers with Cl. Future study on these aspects would greatly aid us to understand the mechanism of ethylene epoxidation.

Bibliography

- [1] *Ethylene Oxide Market — Growth, Trends, COVID -19 Impact, and Forecasts (2021 - 2026)*. en. [Online; accessed 2021-03-22]. URL: <https://www.mordorintelligence.com/industry-reports/ethylene-oxide-market>.
- [2] *Ethylene Oxide Market — Growth, Trends, and Forecast (2020 - 2025)*. en. [Online; accessed 2021-02-09]. URL: <https://www.mordorintelligence.com/industry-reports/ethylene-oxide-market>.
- [3] Tiancheng Pu et al. “Overview of Selective Oxidation of Ethylene to Ethylene Oxide by Ag Catalysts”. en. In: *ACS Catalysis* 9.12 (Dec. 6, 2019), pp. 10727–10750. ISSN: 2155-5435, 2155-5435. DOI: 10.1021/acscatal.9b03443.
- [4] Suljo Linic and Mark A. Barteau. “Formation of a Stable Surface Oxametallacycle that Produces Ethylene Oxide”. In: *Journal of the American Chemical Society* 124.2 (Jan. 1, 2002), pp. 310–317. ISSN: 0002-7863. DOI: 10.1021/ja0118136.
- [5] Suljo Linic and Mark A. Barteau. “Control of Ethylene Epoxidation Selectivity by Surface Oxametallacycles”. In: *Journal of the American Chemical Society* 125.14 (Apr. 1, 2003), pp. 4034–4035. ISSN: 0002-7863. DOI: 10.1021/ja029076g.
- [6] Suljo Linic and Mark A Barteau. “Construction of a reaction coordinate and a microkinetic model for ethylene epoxidation on silver from DFT calculations and surface science experiments”. In: *Journal of Catalysis* 214.2 (2003), pp. 200–212.
- [7] J Will Medlin and Mark A Barteau. “The formation of epoxides from reactions of oxametallacycles on Ag (110): A density functional theory study”. In: *The Journal of Physical Chemistry B* 105.41 (2001), pp. 10054–10061.
- [8] M. Olus Ozbek, Isik Onal, and Rutger A. van Santen. “Ethylene Epoxidation Catalyzed by Silver Oxide”. In: *ChemCatChem* 3.1 (2011). *print* : <https://chemistry-europe.onlinelibrary.wiley.com/doi/pdf/10.1002/cctc.201000249>, pp. 150–153. ISSN: 1867-3899. DOI: <https://doi.org/10.1002/cctc.201000249>.
- [9] M. O. Ozbek and R. A. van Santen. “The Mechanism of Ethylene Epoxidation Catalysis”. en. In: *Catalysis Letters* 143.2 (Feb. 1, 2013), pp. 131–141. ISSN: 1572-879X. DOI: 10.1007/s10562-012-0957-3.
- [10] Charles T Campbell and Bruce E Koel. “Chlorine promotion of selective ethylene oxidation over Ag (110): Kinetics and mechanism”. In: *Journal of Catalysis* 92.2 (1985), pp. 272–283.

- [11] Charles T. Campbell and Mark T. Paffett. “The interactions of O₂, CO and CO₂ with Ag(110)”. en. In: *Surface Science* 143.2 (Aug. 1, 1984), pp. 517–535. ISSN: 0039-6028. DOI: 10.1016/0039-6028(84)90557-0.
- [12] Robert B Grant and Richard M Lambert. “Mechanism of the silver-catalysed heterogeneous epoxidation of ethylene”. In: *Journal of the Chemical Society, Chemical Communications* 12 (1983), pp. 662–663.
- [13] Federico J Williams et al. “Mechanism, selectivity promotion, and new ultras-elective pathways in Ag-catalyzed heterogeneous epoxidation”. In: *Journal of the American Chemical Society* 126.27 (2004), pp. 8509–8514.
- [14] Tulio C.R. Rocha et al. “Promoters in heterogeneous catalysis: The role of Cl on ethylene epoxidation over Ag”. In: *Journal of Catalysis* 312 (2014), pp. 12–16. ISSN: 00219517. DOI: 10.1016/j.jcat.2014.01.002. URL: <http://dx.doi.org/10.1016/j.jcat.2014.01.002>.
- [15] Matthew M Montemore and J Will Medlin. “Predicting and Comparing C–M and O–M Bond Strengths for Adsorption on Transition Metal Surfaces”. In: *The Journal of Physical Chemistry C* 118.5 (2014), pp. 2666–2672.
- [16] Suljo Linic, Jerome Jankowiak, and Mark A Barteau. “Selectivity driven design of bimetallic ethylene epoxidation catalysts from first principles”. In: *Journal of Catalysis* 224.2 (2004), pp. 489–493.
- [17] Peter H. McBreen and Martin Moskovits. “A surface-enhanced Raman study of ethylene and oxygen interacting with supported silver catalysts”. en. In: *Journal of Catalysis* 103.1 (Jan. 1, 1987), pp. 188–199. ISSN: 0021-9517. DOI: 10.1016/0021-9517(87)90105-9.
- [18] Matthew M Montemore et al. “O₂ activation by metal surfaces: implications for bonding and reactivity on heterogeneous catalysts”. In: *Chemical reviews* 118.5 (2017), pp. 2816–2862.
- [19] Geoffrey I. N. Waterhouse, Graham A. Bowmaker, and James B. Metson. “Oxygen chemisorption on an electrolytic silver catalyst: a combined TPD and Raman spectroscopic study”. In: *Applied Surface Science* 214.1 (May 31, 2003), pp. 36–51. ISSN: 0169-4332. DOI: 10.1016/S0169-4332(03)00350-7.
- [20] Chuan-Bao Wang, Goutam Deo, and Israel E. Wachs. “Interaction of Polycrystalline Silver with Oxygen, Water, Carbon Dioxide, Ethylene, and Methanol: In Situ Raman and Catalytic Studies”. In: *The Journal of Physical Chemistry B* 103.27 (July 1, 1999), pp. 5645–5656. ISSN: 1520-6106. DOI: 10.1021/jp9843631.
- [21] D. I. Kondarides et al. “In Situ High Temperature SERS Study of Oxygen Adsorbed on Ag: Support and Electrochemical Promotion Effects”. en. In: *Berichte der Bunsengesellschaft für physikalische Chemie* 97.5 (1993). *eprint* : <https://onlinelibrary.wiley.com/doi/pdf/10.1002/bbpc.19930970511>, pp. 709–719. ISSN: 0005-9021. DOI: 10.1002/bbpc.19930970511.
- [22] Jingfa Deng et al. “In situ surface Raman spectroscopy studies of oxygen adsorbed on electrolytic silver”. In: *Catalysis Letters* 32.1-2 (1995), pp. 159–170. ISSN: 1011372X. DOI: 10.1007/BF00806111.

- [23] Bruno Pettinger et al. “Thermal Decomposition of Silver Oxide Monitored by Raman Spectroscopy: From AgO Units to Oxygen Atoms Chemisorbed on the Silver Surface”. In: *Angewandte Chemie International Edition in English* 33.1 (1994), pp. 85–86. ISSN: 1521-3773. DOI: 10.1002/anie.199400851.
- [24] Emilia A Carbonio et al. “Are multiple oxygen species selective in ethylene epoxidation on silver?” In: *Chemical science* 9.4 (2018), pp. 990–998.
- [25] Wang Xiao-Dong et al. “A reflection-absorption infrared spectroscopy study of the adsorption of atomic oxygen on silver”. en. In: *Surface Science* 257.1 (Nov. 1, 1991), pp. 335–343. ISSN: 0039-6028. DOI: 10.1016/0039-6028(91)90804-2.
- [26] Georg Kresse and Jürgen Furthmüller. “Efficient iterative schemes for ab initio total-energy calculations using a plane-wave basis set”. In: *Physical review B* 54.16 (1996), p. 11169.
- [27] John P Perdew and Yue Wang. “Accurate and simple analytic representation of the electron-gas correlation energy”. In: *Physical review B* 45.23 (1992), p. 13244.
- [28] Georg Kresse and Daniel Joubert. “From ultrasoft pseudopotentials to the projector augmented-wave method”. In: *Physical review b* 59.3 (1999), p. 1758.
- [29] Peter E Blöchl. “Projector augmented-wave method”. In: *Physical review B* 50.24 (1994), p. 17953.
- [30] Anubhav Jain et al. “Commentary: The Materials Project: A materials genome approach to accelerating materials innovation”. In: *APL materials* 1.1 (2013), p. 011002.
- [31] Ask Hjorth Larsen et al. “The atomic simulation environment—a Python library for working with atoms”. en. In: *Journal of Physics: Condensed Matter* 29.27 (June 2017). publisher: IOP Publishing, p. 273002. ISSN: 0953-8984. DOI: 10.1088/1361-648X/aa680e.
- [32] Shyue Ping Ong et al. “Python Materials Genomics (pymatgen): A robust, open-source python library for materials analysis”. en. In: *Computational Materials Science* 68 (Feb. 1, 2013), pp. 314–319. ISSN: 0927-0256. DOI: 10.1016/j.commatsci.2012.10.028.
- [33] Jacob R. Boes and John R. Kitchin. “Neural network predictions of oxygen interactions on a dynamic Pd surface”. In: *Molecular Simulation* 43.5-6 (2017), pp. 346–354. ISSN: 10290435. DOI: 10.1080/08927022.2016.1274984.
- [34] Jacob R. Boes et al. “Graph Theory Approach to High-Throughput Surface Adsorption Structure Generation”. In: *Journal of Physical Chemistry A* 123.11 (2019), pp. 2281–2285. ISSN: 15205215. DOI: 10.1021/acs.jpca.9b00311.
- [35] David Sholl and Janice A Steckel. *Density functional theory: a practical introduction*. John Wiley & Sons, 2011.
- [36] MW Chase et al. “NIST JANAF Thermochemical Tables ver. 1.0”. In: *US Dept. of Commerce* (1985).
- [37] J. E. van den Reijen et al. “Preparation and particle size effects of Ag/-Al₂O₃ catalysts for ethylene epoxidation”. en. In: *Journal of Catalysis* 356 (Dec. 1, 2017), pp. 65–74. ISSN: 0021-9517. DOI: 10.1016/j.jcat.2017.10.001.

- [38] X. Bao et al. “In-situ Raman studies of ethylene oxidation at Ag(111) and Ag(110) under catalytic reaction conditions”. In: *Berichte der Bunsengesellschaft Physical Chemistry Chemical Physics* 97.3 (1993), pp. 322–325. ISSN: 00059021. DOI: 10.1002/bbpc.19930970312.
- [39] X. Bao et al. “The effect of water on the formation of strongly bound oxygen on silver surfaces”. en. In: *Catalysis Letters* 32.1 (Mar. 1, 1995), pp. 171–183. ISSN: 1572-879X. DOI: 10.1007/BF00806112.
- [40] Radwan Abdallah et al. “(54) PROCESS FOR MAKING ETHYLENE OXDE”. en. In: (), p. 20.
- [41] Saharley WNU. “(75) Inventors: Liping Zhang, Lake Jackson, TX (US); Ravindra Radhakisan Tupe, Heisinki (FI); Ailene Gardner Phillips, Charleston, WV (US); Paul Victor”. en. In: (), p. 19.
- [42] E Force and Alexis T. Bell. “The relationship of adsorbed species observed by infrared spectroscopy to the mechanism of ethylene oxidation over silver”. en. In: *Journal of Catalysis* 40.3 (Dec. 1975), pp. 356–371. ISSN: 00219517. DOI: 10.1016/0021-9517(75)90267-5.
- [43] Valerii I. Bukhtiyarov et al. “Combined in situ XPS and PTRMS study of ethylene epoxidation over silver”. en. In: *Journal of Catalysis* 238.2 (Mar. 10, 2006), pp. 260–269. ISSN: 0021-9517. DOI: 10.1016/j.jcat.2005.11.043.
- [44] Travis E. Jones et al. “Thermodynamic and spectroscopic properties of oxygen on silver under an oxygen atmosphere”. In: *Physical Chemistry Chemical Physics* 17.14 (2015), pp. 9288–9312. ISSN: 14639076. DOI: 10.1039/c5cp00342c.
- [45] Travis E. Jones et al. “Insights into the Electronic Structure of the Oxygen Species Active in Alkene Epoxidation on Silver”. In: *ACS Catalysis* 5.10 (Oct. 2, 2015). publisher: American Chemical Society, pp. 5846–5850. DOI: 10.1021/acscatal.5b01543.
- [46] Graeme J. Millar et al. “In situ Raman studies of the selective oxidation of methanol to formaldehyde and ethene to ethylene oxide on a polycrystalline silver catalyst”. en. In: *Journal of the Chemical Society, Faraday Transactions* 91.22 (1995). publisher: Royal Society of Chemistry, pp. 4149–4159. DOI: 10.1039/FT9959104149.
- [47] Angeles Pulido et al. “Aerobic epoxidation of propene over silver (1 1 1) and (1 0 0) facet catalysts”. In: *Journal of catalysis* 292 (2012), pp. 138–147.
- [48] Suljo Linic and Mark A. Barteau. “On the Mechanism of Cs Promotion in Ethylene Epoxidation on Ag”. In: *Journal of the American Chemical Society* 126.26 (July 1, 2004), pp. 8086–8087. ISSN: 0002-7863. DOI: 10.1021/ja048462q.
- [49] Charles T. Campbell. “The selective epoxidation of ethylene catalyzed by Ag(111): A comparison with Ag(110)”. en. In: *Journal of Catalysis* 94.2 (Aug. 1, 1985), pp. 436–444. ISSN: 0021-9517. DOI: 10.1016/0021-9517(85)90208-8.
- [50] Charles T. Campbell. “Atomic and molecular oxygen adsorption on Ag(111)”. en. In: *Surface Science* 157.1 (July 1, 1985), pp. 43–60. ISSN: 0039-6028. DOI: 10.1016/0039-6028(85)90634-X.

- [51] Weijian Diao et al. “An investigation on the role of Re as a promoter in AgCsRe/-Al₂O₃ high-selectivity, ethylene epoxidation catalysts”. en. In: *Journal of Catalysis* 322 (Feb. 1, 2015), pp. 14–23. ISSN: 0021-9517. DOI: 10.1016/j.jcat.2014.11.007.
- [52] Cha Jung Chen, James W. Harris, and Aditya Bhan. “Kinetics of Ethylene Epoxidation on a Promoted Ag/ α -Al₂O₃Catalyst—The Effects of Product and Chloride Co-Feeds on Rates and Selectivity”. In: *Chemistry - A European Journal* 24.47 (2018), pp. 12405–12415. ISSN: 15213765. DOI: 10.1002/chem.201801356.
- [53] James W. Harris and Aditya Bhan. “Moderation of chlorine coverage and ethylene epoxidation kinetics via ethane oxychlorination over promoted Ag/-Al₂O₃”. In: *Journal of Catalysis* 367 (2018), pp. 62–71. ISSN: 10902694. DOI: 10.1016/j.jcat.2018.08.021. URL: <https://doi.org/10.1016/j.jcat.2018.08.021>.
- [54] N. M. Martin et al. “High-coverage oxygen-induced surface structures on Ag(111)”. In: *Journal of Physical Chemistry C* 118.28 (2014), pp. 15324–15331. ISSN: 19327455. DOI: 10.1021/jp504387p.
- [55] C. I. Carlisle et al. “Imaging the surface and the interface atoms of an oxide film on Ag(111) by scanning tunneling microscopy: Experiment and theory”. In: *Physical Review Letters* 84.17 (2000), pp. 3899–3902. ISSN: 10797114. DOI: 10.1103/PhysRevLett.84.3899.
- [56] Angelos Michaelides, Karsten Reuter, and Matthias Scheffler. “When seeing is not believing: Oxygen on Ag(111), a simple adsorption system?” In: *Journal of Vacuum Science Technology A: Vacuum, Surfaces, and Films* 23.6 (2005), pp. 1487–1497. ISSN: 0734-2101. DOI: 10.1116/1.2049302.
- [57] M. Pascal et al. “Photoelectron diffraction study of the Ag(110)-(2 \times 1)-O reconstruction”. In: *Surface Science* 464.2-3 (2000), pp. 83–90. ISSN: 00396028. DOI: 10.1016/S0039-6028(00)00669-5.
- [58] G. Dorenbos and D. O. Boerma. “The structure of the Ag(110)-c(6 \times 2)O surface determined with LEIS”. In: *Surface Science* 287-288.PART 1 (1993), pp. 443–447. ISSN: 00396028. DOI: 10.1016/0039-6028(93)90820-A.
- [59] G Bracco and R Tatarek. “The missing-row-reconstructed p (3 \times 1) O-Ag (110) surface”. In: *Surface science* 251 (1991), pp. 498–502.
- [60] Charles T Campbell and Mark T Paffett. “Model studies of ethylene epoxidation catalyzed by the Ag (110) surface”. In: *Surface science* 139.2-3 (1984), pp. 396–416.
- [61] I. Costina et al. “Combined STM, LEED and DFT study of Ag(1 0 0) exposed to oxygen near atmospheric pressures”. In: *Surface Science* 600.3 (2006), pp. 617–624. ISSN: 00396028. DOI: 10.1016/j.susc.2005.11.020.
- [62] Wei Xue Li, Catherine Stampfl, and Matthias Scheffler. “Oxygen adsorption on Ag(111): A density-functional theory investigation”. In: *Physical Review B - Condensed Matter and Materials Physics* 65.7 (2002). ISSN: 1550235X. DOI: 10.1103/PhysRevB.65.075407.

- [63] Jonathan Derouin et al. “Formation of surface oxides and Ag₂O thin films with atomic oxygen on Ag(111)”. In: *Surface Science* 641 (2015), pp. L1–L4. ISSN: 00396028. DOI: 10.1016/j.susc.2015.07.003.
- [64] Christian Heine et al. “A study of the O/Ag(111) system with scanning tunneling microscopy and x-ray photoelectron spectroscopy at ambient pressures”. In: *Surface Science* 652 (2016), pp. 51–57. ISSN: 00396028. DOI: 10.1016/j.susc.2016.02.012.
- [65] M. Oluş Özbek, Işık Önal, and Rutger A. VanSanten. “Chlorine and Caesium Promotion of Silver Ethylene Epoxidation Catalysts”. In: *ChemCatChem* 5.2 (2013), pp. 443–451. ISSN: 18673880. DOI: 10.1002/cctc.201200690.